Mon. Not. R. Astron. Soc. **000**, 1–10 () Printed 1 December 2000 (MN LATEX style file v1.4)

Simple dynamical models of the Sagittarius dwarf galaxy

Amina Helmi[1,2,3] and Simon D.M. White[2]
[1] *Sterrewacht Leiden, Postbus 9513, 2300 RA Leiden, The Netherlands*
[2] *Max-Planck-Institut für Astrophysik, Karl-Schwarzschild-Str. 1, 85740 Garching bei München, Germany*
[3] *Observatorio Astronómico de La Plata, Paseo del Bosque s/n, B1900FWA La Plata, Argentina*

Accepted ... Received ...; in original form ...

ABSTRACT
We present two simple dynamical models for Sagittarius based on N-body simulations of the progressive disruption of a satellite galaxy orbiting for 12.5 Gyr within a realistic Galactic potential. In both models the satellite initially has observable properties similar to those of current outlying dwarfs; in one case it is purely stellar while in the other it is embedded in an extended massive halo. The purely stellar progenitor is a King model with a total velocity dispersion of 18.9 $\mathrm{km\,s^{-1}}$, a core radius of 0.44 kpc and a tidal radius of 3 kpc. The initial stellar distribution in the other case follows a King profile with the same core radius, a slightly larger total velocity dispersion and similar extent. Both these models are consistent with all published data on the current Sagittarius system, they match not only the observed properties of the main body of Sagittarius, but also those reported for unbound debris at larger distances.

Key words: galaxies: interactions, individual (Sagittarius dSph), Local Group – Galaxy: halo, structure

1 INTRODUCTION

The Sagittarius dwarf galaxy is the closest satellite of the Milky Way (Ibata, Gilmore & Irwin 1994, 1995, hereafter IGI95). Soon after its discovery, several groups carried out simulations to see if its properties are consistent with the disruption of an object similar to the other dwarf companions of the Milky Way, but none produced a model in full agreement with both the age and the structure of the observed system (Johnston, Spergel & Hernquist 1995; Velázquez & White 1995; Edelsohn & Elmegreen 1997; Ibata et al. 1997, hereafter I97; Gómez-Flechoso, Fux & Martinet 1999). All groups assumed light to trace mass and an initial system similar to observed dwarf spheroidals. All found the simulated galaxy to disrupt after one or two orbits whereas the observed system has apparently completed ten or more. Most considered this to be a problem (but cf Velázquez & White 1995). As a result, several unconventional models were proposed to explain the survival and structure of Sagittarius. In an extensive numerical study, Ibata & Lewis (1998) concluded that Sagittarius must have a stiff and extended dark matter halo if it is to survive with 25% of its initial mass still bound today. Since an extended halo cannot remain undistorted in the Galaxy's tidal field for any conventional form of dark matter, it is unclear how this idea should be interpreted. Furthermore, it produces an uncomfortably large mass-to-light ratio (~ 100), it cannot reproduce the observed elongation, and it suggests that little tidal debris will be liberated, in apparent conflict with the observations of Mateo, Olszewski & Morrison (1998), and Majewski et al. (1999) (see also Johnston et al. 1999). A somewhat less unorthodox model was proposed by Zhao (1998), where Sagittarius was scattered onto its current tightly bound orbit by an encounter with the Magellanic Clouds about 2 Gyr ago. This appears physically possible but requires careful tuning of the orbits of the two systems (see Ibata & Lewis 1998; and Jiang & Binney 2000). Another mechanism by which the dwarf could have moved to a short-period orbit is dynamical friction, which can be important only if Sagittarius has lost a lot of mass in the past. Jiang & Binney (2000) found a one-parameter family of initial configurations that evolve into something like the present system over a Hubble time. Their initial systems have masses $\sim 10^{10-11}\,\mathrm{M}_\odot$ and start from a Galactocentric radius ~ 200 kpc.

Driven by this apparent puzzle, we decided to search more thoroughly for a self-consistent model of the disruption of Sagittarius, which, after a Hubble time, has similar characteristics to those observed. (See Table 1 for a summary of the observed properties of the system.) Below we present two models which meet these requirements.

2 METHOD

In our numerical simulations, we represent the Galaxy by a fixed potential with three components: a dark logarithmic halo

$$\Phi_{\mathrm{halo}} = v_{\mathrm{halo}}^2 \ln(r^2 + d^2), \tag{1}$$

Table 1. Properties of Sagittarius (IGI95, I97)

Orbital properties	
distance from the Sun d	25 ± 2 kpc
heliocentric radial velocity $v_r^{\rm sun}$	$140 \pm 2\,{\rm km\,s^{-1}}$
proper motion in b μ_b	$250 \pm 90\,{\rm km\,s^{-1}}$
gradient along the orbit ${\rm d}v_r/{\rm d}b$	$< 3\,{\rm km\,s^{-1}}/\,{\rm deg}$
angular position in the sky (l, b)	$(5.6°, -14°)$
Internal properties	
luminosity	$\gtrsim 10^7\,{\rm L_\odot}$
velocity dispersion $\sigma(v_r)$	$11.4 \pm 1\,{\rm km\,s^{-1}}$
angular extent in (l, b)	$8° \times 3°$
half-mass radius	0.55 kpc
mean metallicity $\langle[{\rm Fe/H}]\rangle$	$\sim -1.$ dex

a Miyamoto-Nagai disk

$$\Phi_{\rm disk} = -\frac{GM_{\rm disk}}{\sqrt{R^2 + (a + \sqrt{z^2 + b^2})^2}}, \qquad (2)$$

and a spherical Hernquist bulge

$$\Phi_{\rm bulge} = -\frac{GM_{\rm bulge}}{r + c}, \qquad (3)$$

where d=12 kpc and $v_{\rm halo} = 131.5\ {\rm km\,s^{-1}}$; $M_{\rm disk} = 10^{11}\,{\rm M_\odot}$, $a = 6.5$ kpc and $b = 0.26$ kpc; $M_{\rm bulge} = 3.4 \times 10^{10}\,{\rm M_\odot}$ and $c = 0.7$ kpc. This choice of parameters gives a flat rotation curve with an asymptotic circular velocity of 186 ${\rm km\,s^{-1}}$. The mass of the dark-matter halo within 16 kpc is 7.87 $\times 10^{10}\,{\rm M_\odot}$ in this model.

We represent the satellite galaxy by a collection of 10^5 particles and model their self-gravity by a multipole expansion of the internal potential to fourth order (White 1983; Zaritsky & White 1988). This type of code has the advantage that a large number of particles can be followed in a relatively small amount of computer time. Hence a substantial parameter space can be explored while retaining considerable detail on the structure of the disrupted system. In this quadrupole expansion, higher than monopole terms are softened more strongly. We choose $\epsilon_1 \sim 0.2 - 0.25 r_c$ for the monopole term (r_c is the core radius of the system) and $\epsilon_2 = 2\epsilon_1$ for dipole and higher terms and for the centre of expansion. The centre of expansion is a particle which, in practice, follows the density maximum of the satellite closely at all times.

For the stellar distribution of the pre-disruption dwarf we choose a King model (King 1966), since this is a good representation of the distant dwarf spheroidals. King models are defined by a combination of three parameters: $\Psi(r=0)$ (depth of the potential well of the system), σ^2 (measure of the central velocity dispersion), and ρ_0 (central density) or r_0 (King radius). The ratio $\Psi(r=0)/\sigma^2$ defines how centrally concentrated the system is, and for any value of this parameter, a set of homologous models with different central densities and core (or King) radii may be found. We assume that the progenitor of Sagittarius obeys the known metallicity-luminosity relation for the Local Group dSph (Mateo 1998). The metallicity determinations for Sagittarius (I97) indicate $\langle[{\rm Fe/H}]\rangle \sim -1$, corresponding to a *total* luminosity in the range $3.5 \times 10^7 - 3.5 \times 10^8\,{\rm L_\odot}$. To obtain an initial guess for the mass of the system, we transform this luminosity into a mass assuming a mass-to-light ratio ~ 2. The relevant initial stellar mass interval is then $7 \times 10^7 - 7 \times 10^8\,{\rm M_\odot}$.

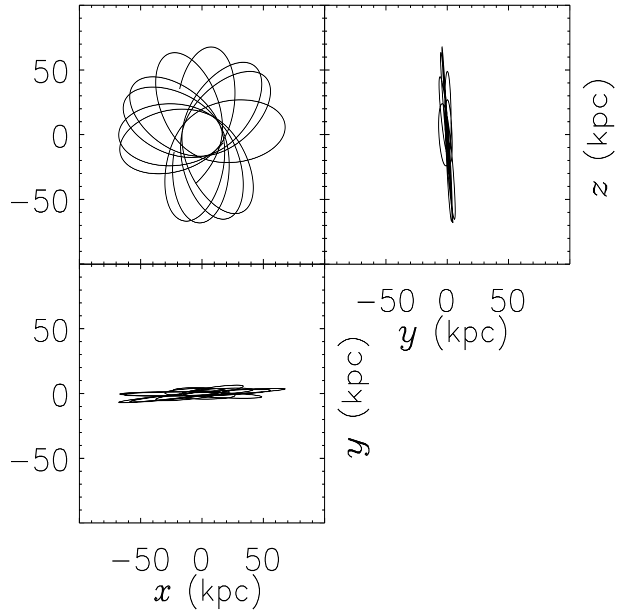

Figure 1. Projections of a possible orbit of Sagittarius on different orthogonal planes, where xy coincides with the plane of the Galaxy.

Note that our choice of a fixed potential to represent our Galaxy means that we neglect any exchange of energy between the satellite and the Galactic halo. This is an excellent approximation for the range of orbits and satellite masses that we consider, since these imply dynamical friction decay times substantially in excess of the Hubble time. The orbits are also sufficiently large that impulsive heating during disk passages can be neglected.

The orbit of Sagittarius is relatively well constrained (I97). The heliocentric distance $d \sim 25 \pm 2$ kpc and position $(l, b) = (5.6°, -14°)$ of the galaxy core are well-determined; the heliocentric radial velocity $v_r^{\rm sun} \sim 140 \pm 2\,{\rm km\,s^{-1}}$, and its variation across the satellite are also accurately measured. Outside the main body ($b < -20°$) the radial velocity shows a small gradient ${\rm d}v_r/{\rm d}b \lesssim 3\,{\rm km\,s^{-1}}$ deg, but no gradient is detected across the main body itself. The proper motion measurements are not very accurate; $\mu_b \sim 2.1 \pm 0.7 {\rm mas\,yr^{-1}}$, and no measurement is available in the l-direction. On the other hand the strong North-South elongation of the system suggests that it has little motion in the l-direction, thus implying the orbit should be close to polar. We generate a range of possible orbits satisfying these constraints and concentrate on those with relatively long periods in order to maximise the survival chances of our satellite. We begin all our simulations half a radial period after the Big Bang to allow for the initial expansion. We place the initial satellite at apocentre, then we integrate forward until ~ 13 Gyr. The orbits are chosen so at this time the position and velocity of the satellite core correspond to those observed. We allow ourselves some slight freedom in choosing the final time in order to fit the observed data as well as possible.

3 RESULTS

Figure 1 gives an example of an orbit which is consistent with all the current data on Sagittarius. It has a pericentre of 16.3 kpc, an apocentre of 68.3 kpc, and a radial period of ~ 0.85 Gyr. We use similar orbits for all the simulations described below. Note that the slow precession about the Galactic rotation axis is in part due to the quasi-polar nature of the orbit and in part to the fact we have assumed the Milky Way's dark halo to be spherical.

After letting our satellite relax in isolation, we integrate each simulation for ~ 13 Gyr. In practice we needed to run a large number of simulations, and test each to see if it satisfies the observational constraints at the present time. Since it remains uncertain whether dwarf spheroidals have extended dark halos (e.g. Klessen & Kroupa 1998), we have considered both purely stellar models and models in which the initial stellar system is embedded in a more massive and more extended dark halo.

3.1 Constant mass-to-light ratio: A purely stellar model

Our preferred purely stellar model (Model I) initially has a core radius of $r_c = 0.44$ kpc, a total velocity dispersion of 18.9 $\mathrm{km\,s^{-1}}$, and a concentration parameter $c = \log_{10}(r_t/r_c) \sim 0.83$. This implies a total mass of $M = 4.66 \times 10^8\,\mathrm{M_\odot}$. For a satellite to survive for about 10 Gyr on an orbit with pericentre ~ 15 kpc, apocentre ~ 70 kpc, and period ~ 1 Gyr (for which the observational constraints are satisfied) its initial central density has to be $\rho_0 \geq 0.36 - 0.4\,\mathrm{M_\odot pc^{-3}}$. Satellites with significantly smaller initial densities do not survive long enough.

In Figure 2 we plot heliocentric distance as a function of galactic latitude for stars projected near the main remnant 12.5 Gyr after infall. Streams of particles are visible at all latitudes over a broad range in distance. Sagittarius has been orbiting long enough for its debris streams to be wrapped several times around the Galaxy. (See also Figure 8.)

The remnant galaxy, i.e. the central region of the satellite's debris, is similar to the real system. In Figure 3 we plot its mass surface density. The transformation from observed surface brightness to mass surface density (which is what the simulations give us) can be done as follows. The observed mass surface density Σ for an assumed mass-to-light ratio Υ is

$$\Sigma = \frac{N_X L_X}{f_X}\Upsilon \qquad \left[\frac{\mathrm{M_\odot}}{\mathrm{deg}^2}\right], \tag{4}$$

where N_X is the number of observed stars of type X per square degree, L_X is their luminosity, and f_X is the fraction of the total luminosity in stars of type X. In IGI95 the spatial structure of Sagittarius was determined from the excess of counts at the apparent magnitude of the horizontal branch. Uncertainties in the result are due primarily to contamination by sources in the Galactic bulge. Their lowest isodensity contour is at $\Sigma_{\mathrm{min}} \sim 5 \times 10^5 \frac{\mathrm{M_\odot}}{\mathrm{deg}^2}$, assuming $\Upsilon \sim 2.25$ and [Fe/H] ~ -1 (Bergbusch & vandenBerg 1992), and has an extent of $7.5^\circ \times 3^\circ$. This same isodensity contour is shown in Figure 3 as a thick line. It has an extent of $\sim 8^\circ \times 4.8^\circ$, in reasonable agreement with the observations given the uncertainties. In I97 isodensity contours were derived from counts of main sequence stars close to the turn-off, roughly one magnitude above the plate limit. The minimum contour in this case corresponds to $\Sigma_{\mathrm{min}} \sim 10^5 \frac{\mathrm{M_\odot}}{\mathrm{deg}^2}$, and has an extent of roughly $15^\circ \times 7^\circ$. In Fig. 3 this contour is shown as a dashed-line, and has an extent of $21^\circ \times 6.5^\circ$, also in good agreement with the observations. Note that the isophotes (or isodensity contours) become rounder towards the centre of the satellite. Its angular core radius is $R_c \sim 1.29^\circ$, which for a distance of 26 kpc (derived from the simulations) corresponds to 0.58 kpc, again in good agreement with the observations.

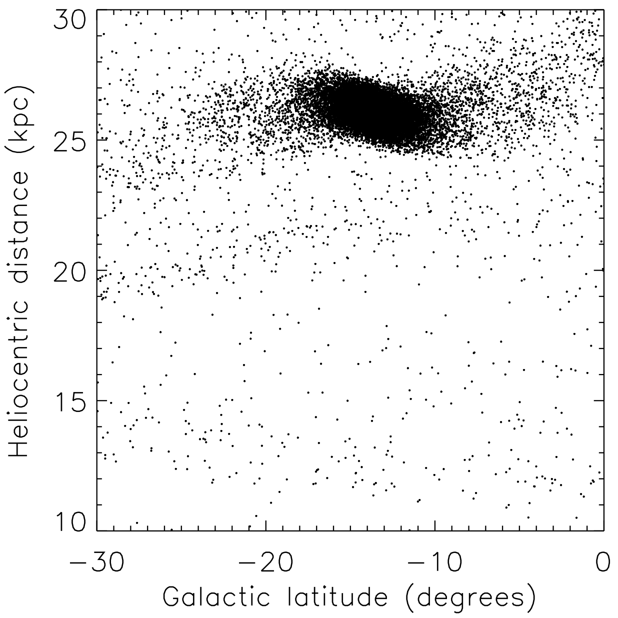

Figure 2. Distribution of particles in distance from the Sun as a function of latitude. For direct comparison see Figure 4 of I97.

The kinematic properties of the remnant galaxy are more difficult to compare with observations because a substantial amount of mass from debris streams is projected on top of the main body. Like I97, we measure the radial velocity across the system considering only particles for which $100\,\mathrm{km\,s^{-1}} \leq v_r^{\mathrm{sun}} \leq 180\,\mathrm{km\,s^{-1}}$. In the left panel of Figure 4 we plot the heliocentric radial velocity, and in the right panel we plot its dispersion as a function of Galactic latitude. For comparison, we analysed the observations of I97 at CTIO in the same way (their Table 2b); these data have a precision of a few $\mathrm{km\,s^{-1}}$ (triangles in Figure 4). Our model is consistent with the observed kinematics; we obtain a heliocentric radial velocity of $139.5\,\mathrm{km\,s^{-1}}$ and an internal velocity dispersion in the radial direction of $11\,\mathrm{km\,s^{-1}}$ for the main body. However, when the radial velocity restrictions for inclusion in this calculation are relaxed, we find much larger velocity dispersions because of the contribution of stars from other streams. It is important to consider this problem when determining which stars should be considered members of Sagittarius.

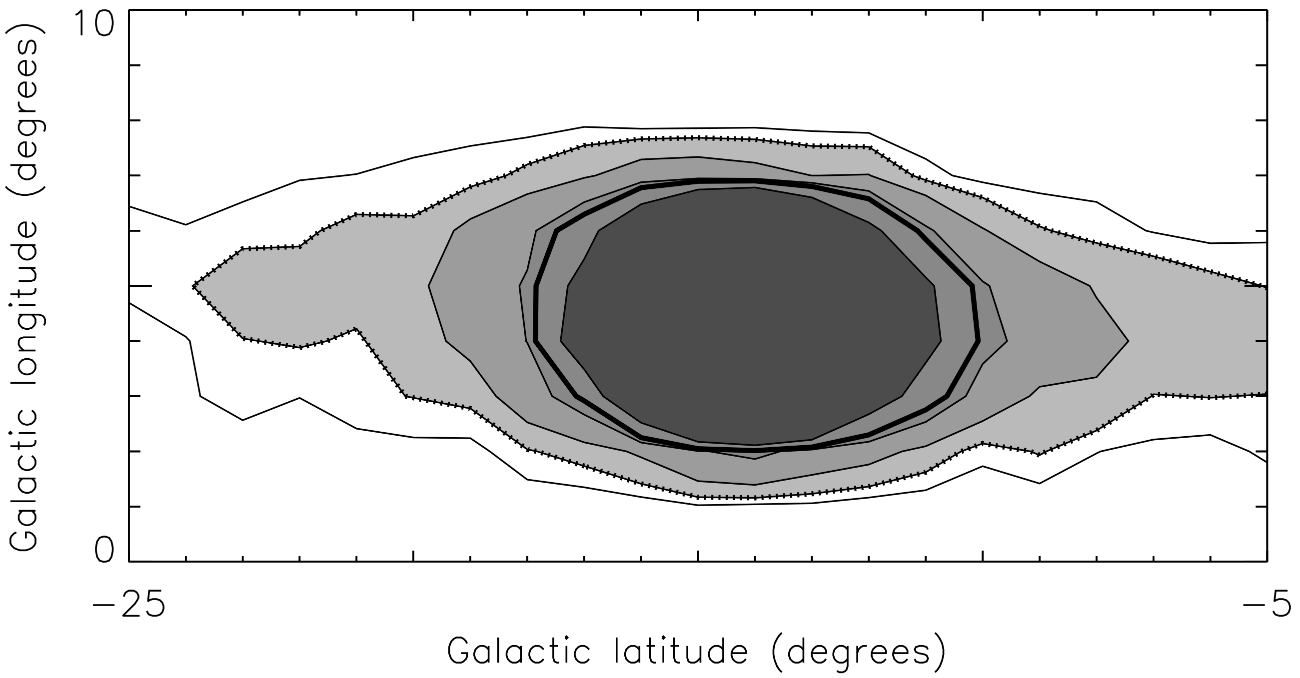

Figure 3. Surface isodensity contours for the remnant system. The thick and dashed lines indicate the contours that, for $M/L = 2.25$, would correspond to the minimum contours plotted in 1994 and in 1997 respectively by Ibata and collaborators. Each succeeding contour has half the mass surface density of the previous one.

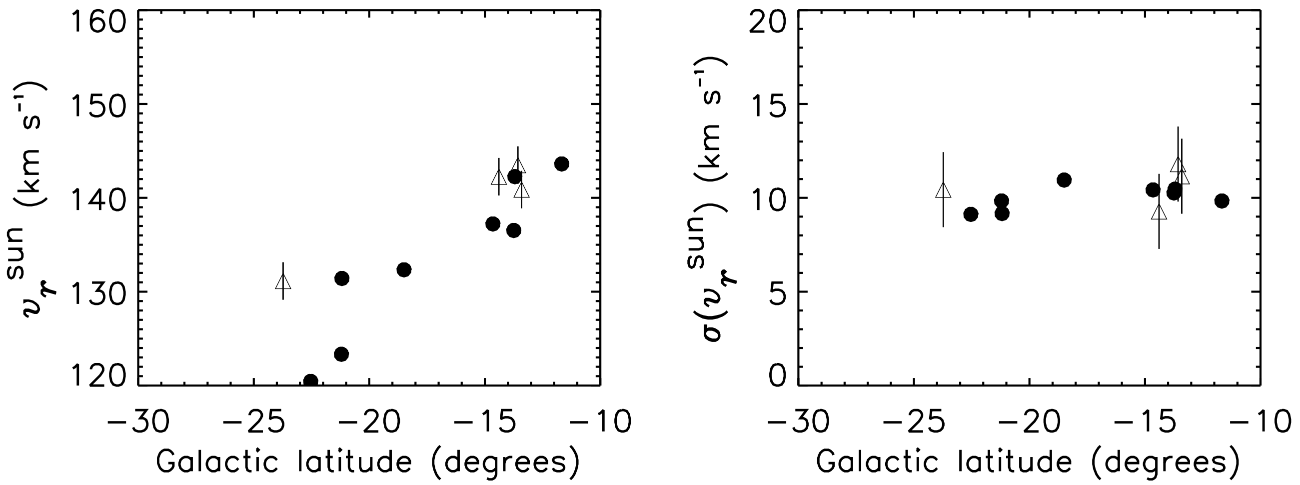

Figure 4. In the left panel we plot mean heliocentric radial velocity as a function of Galactic latitude, for bins of $\sim 2.5° \times 2.5°$ across the remnant system. The right panel shows the heliocentric radial velocity dispersion in the same bins. To determine variations across the main body of the galaxy, we have taken bins centered on the same Galactic latitude but offset in Galactic longitude. The triangles correspond to data from I97, error bars indicate 2 $\mathrm{km\,s^{-1}}$ uncertainty.

3.2 Varying mass-to-light ratio: A model with a dark halo

The observational data for Sagittarius mainly refer to the current remnant system, which corresponds to the innermost regions of the progenitor satellite. As a consequence, models that are initially dark matter dominated in their outskirts are relatively poorly constrained.

As an example we focus on a progenitor with a mass distribution which is similar to that of Model I in its inner regions, but is considerably more extended. We take the mass distribution to be a (heavy) King model with $r_c = 0.54$ kpc and $r_t = 10.4$ kpc, with an initial total velocity dispersion of 25.2 $\mathrm{km\,s^{-1}}$, and total mass of $M = 1.7 \times 10^9\ \mathrm{M}_\odot$. For an orbit like that of Model I this produces a suitable remnant after 12 Gyr. The *mass* distribution of this remnant satisfies many of the observational constraints of Table 1. Its core radius is slightly larger $r_c \sim 0.65$ kpc, and the radial velocity dispersion in the main body is 12.1 $\mathrm{km\,s^{-1}}$.

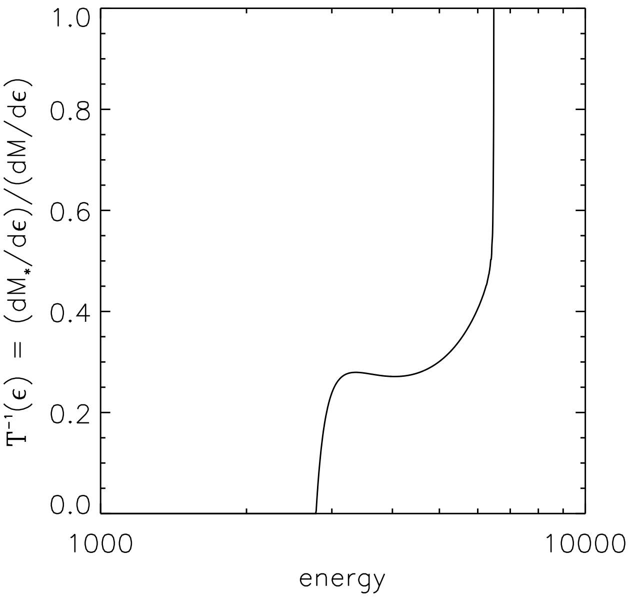

Figure 5. Inverse mass-to-light ratio as a function of binding energy for our model II. Negative values of the energy correspond to unbound material. Particles in the deepest parts of the potential well have stellar mass-to-light ratios.

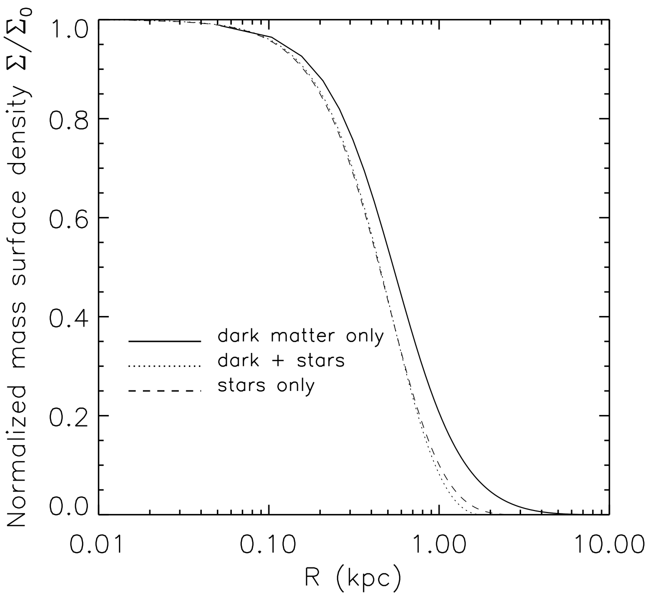

Figure 6. The dashed curve corresponds to the surface density of Model I normalized to its central value ($\Sigma_0 = 7.29\times10^2$ M$_\odot$/pc^2). The solid curve to that of the heavy King model, which corresponds to the total mass of Model II ($\Sigma_0 = 11.17\times10^2$ M$_\odot$/pc^2). Model II, obtained by weighting each simulation particle by $(M/L)^{-1}$, is shown as the dotted curve. Model I and Model II have almost the same surface density profile by construction.

We will construct a two-component satellite with this mass distribution by solving for the dependence of mass-to-light ratio on initial binding energy that produces the initial light profile of Model I. We choose the mass-to-light ratio of satellite material to be a decreasing function of binding energy, so that the most bound particles have near "stellar" mass-to-light ratios, whereas weakly bound particles are almost entirely "dark". From the energy distribution of the heavy King model, and that of a King model with $r_0 = 0.095$ kpc and $\sigma = 25.6\,\mathrm{km\,s^{-1}}$, we can derive the mass-to-light ratio as a function of binding energy as

$$\Upsilon(\epsilon) = \Upsilon_* \frac{\mathrm{d}M/\mathrm{d}\epsilon(\epsilon)}{\mathrm{d}M_*/\mathrm{d}\epsilon(\epsilon = \epsilon_* + \epsilon_{\max} - \epsilon_{*\max})} \tag{5}$$

where Υ_* is the mass-to-light ratio of a stellar population. The energies ϵ_* of the lighter King model have been shifted by a fixed amount $\epsilon_{\max} - \epsilon_{*\max}$, to be on the same scale as that of the heavier King model. The resulting mass-to-light ratio is shown in Figure 5.

In Figure 6 we show the surface mass densities normalized to their central values for Model I (only stars), for the heavy King model and for the two-component model ("stars" and dark-matter). We shall refer to this two-component model as Model II, which is obtained by weighting each simulation particle by $\Upsilon(\epsilon)^{-1}$.

If we require that the central stellar mass surface densities of Model I and Model II be the same, we find that the total mass in stars in Model II is $\sim 1.69\times10^8$ M$_\odot$. To match Sagittarius surface brightness, we choose the central stellar mass-to-light ratio $\Upsilon_* = 1.5$. Thus, the total luminosity of Model II is then 1.13×10^8 L$_\odot$, implying a mass-to-light ratio of 15.1. Its initial velocity dispersion is 23 $\mathrm{km\,s^{-1}}$. The visible extent of the remnant has properties which are almost identical to those of Model I, and we find its velocity dispersion to be $11.1\,\mathrm{km\,s^{-1}}$. Both results are again in good agreement with the observations.

The two initial satellites (Models I and II) have the same stellar mass distributions in their inner regions, differing only in that one has an extended dark halo. We may thus conclude that the presence of a dark halo does not affect the final structure of the remnant, which is very similar in both models. However there is a significant difference in the properties of their debris streams. In Model I the unbound debris streams are predicted to contain 5.2 times the light in the main body of the remnant ($M_V \sim -14.1$), as defined by the dotted contour in Figure 3, whereas in Model II ($M_V \sim -13.4$) this ratio is 4.85. If we had chosen Model II to be a constant mass-to-light ratio model, we would have got an almost equally good fit to the main body of Sagittarius, but would have predicted the streams to contain 19 times the light in the main body of the remnant. In this last case, Sagittarius would have contributed 4.56×10^8 L$_\odot$ to the Galactic stellar halo in the form of debris stars (for $\Upsilon = 3.5$). Thus we see that the observed properties of the main remnant do not usefully constrain the number of stars that may be present in the debris streams, but that the different models can be better constrained from the properties of their debris streams, as we exemplify below.

3.3 Discussion

3.3.1 Some predictions

In this section we concentrate for simplicity on Model I. We can use it to predict star counts as a function of distance and radial velocity at different points on the sky. We focus on fields along the path defined by the orbit of Sgr, which is where we expect to find debris streams. This is illustrated in Figure 7, where the number counts are normalized to their

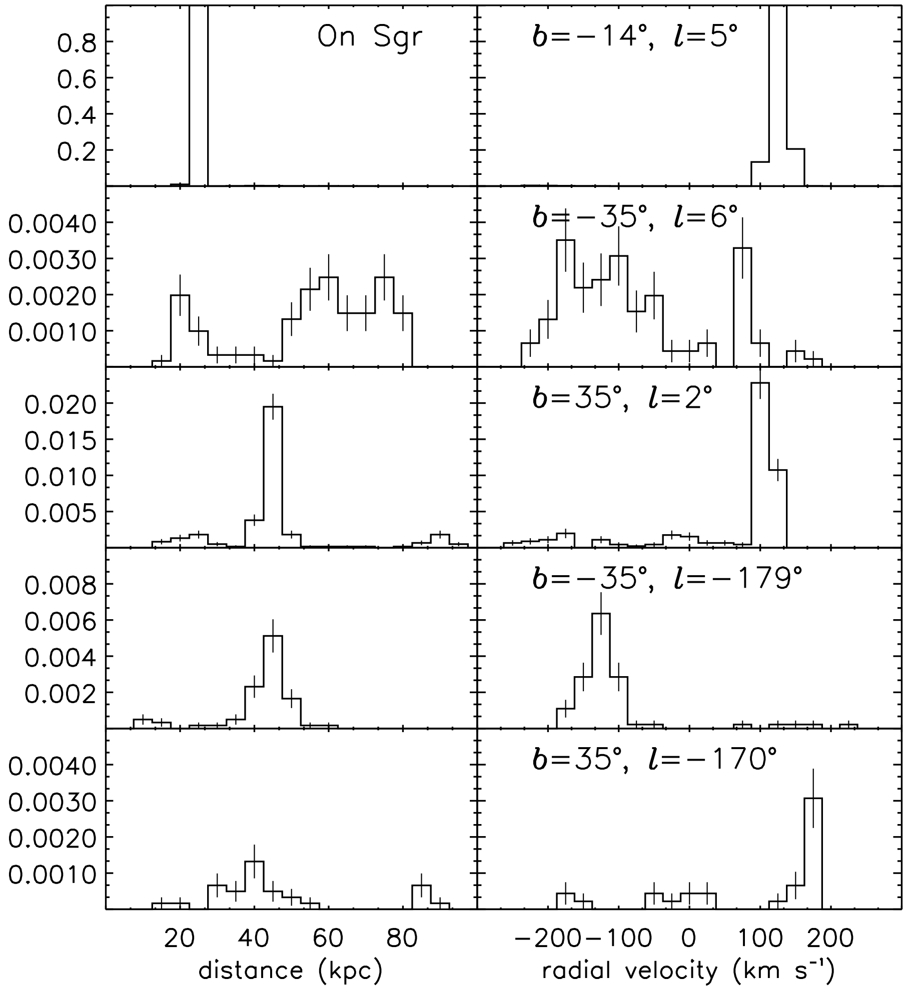

Figure 7. Number counts in 1×1 deg^2 normalized to the main body of Sagittarius, which is shown in the top row. Distance bins are 5 kpc, and radial velocity bins are $25\,\mathrm{km\,s^{-1}}$. All quantities are heliocentric. Note that the debris reaches larger densities, and could thus be more easily detectable, at $b \sim 35°$ for the stream in the Galactic centre direction, and $b \sim -35°$ for the anticentre stream.

values on the main body of our simulated Sagittarius, as shown in the first row. We assume fields which are $1° \times 1°$. For the distance, we use 5 kpc bins, whereas for the radial velocity we take 25 $\mathrm{km\,s^{-1}}$ bins. Note that the contrast of structures in the radial velocity counts are generally larger than in the distance counts, indicating that it should be easier to detect streams in velocity space rather than as density inhomogeneities (see also Helmi & White 1999). This is particularly true considering the much greater relative precision of the velocity measurements. Space density enhancements often occur near the orbital turning points; several are seen as sharp features in the central panel of Fig. 8.

Our model can also be used to predict where streams originating in different mass loss events should be found. This is illustrated in Figure 8 where different colours indicate material lost at different pericentric passages. Note that since the surface brightness of the unbound material decreases with time, material lost in early passages is considerably more difficult to detect than recent mass loss (for an axisymmetric potential the time dependence is $1/t^2$, but if the potential may be considered as nearly spherical the surface density will effectively decrease as $1/t$; see Helmi & White 1999). The central panel (latitude vs. heliocentric distance) explains why Sagittarius streams have been more difficult to detect above the Galactic plane than below it, even though the density contrast is higher for the northern streams (as shown in the second and third panels of Fig. 7). From the left panel, $-90° \le l \le 90°$, we see that the stream of stars lost in the previous pericentric passage (shown in blue) becomes more distant as we go north. For example, at $b = 40°$, the stream is located approximately 50 kpc from the Sun. The red giant clump visual magnitude at this distance would be roughly 19.3^m, compared to the 17.85^m observed in the main body of Sagittarius.

3.3.2 *Comparison to data outside the main body of Sagittarius*

Even though we have constructed our models to reproduce the properties of the main body of Sagittarius, it is nevertheless worthwhile to compare our simulations to data sets which have claimed detections of Sagittarius debris.

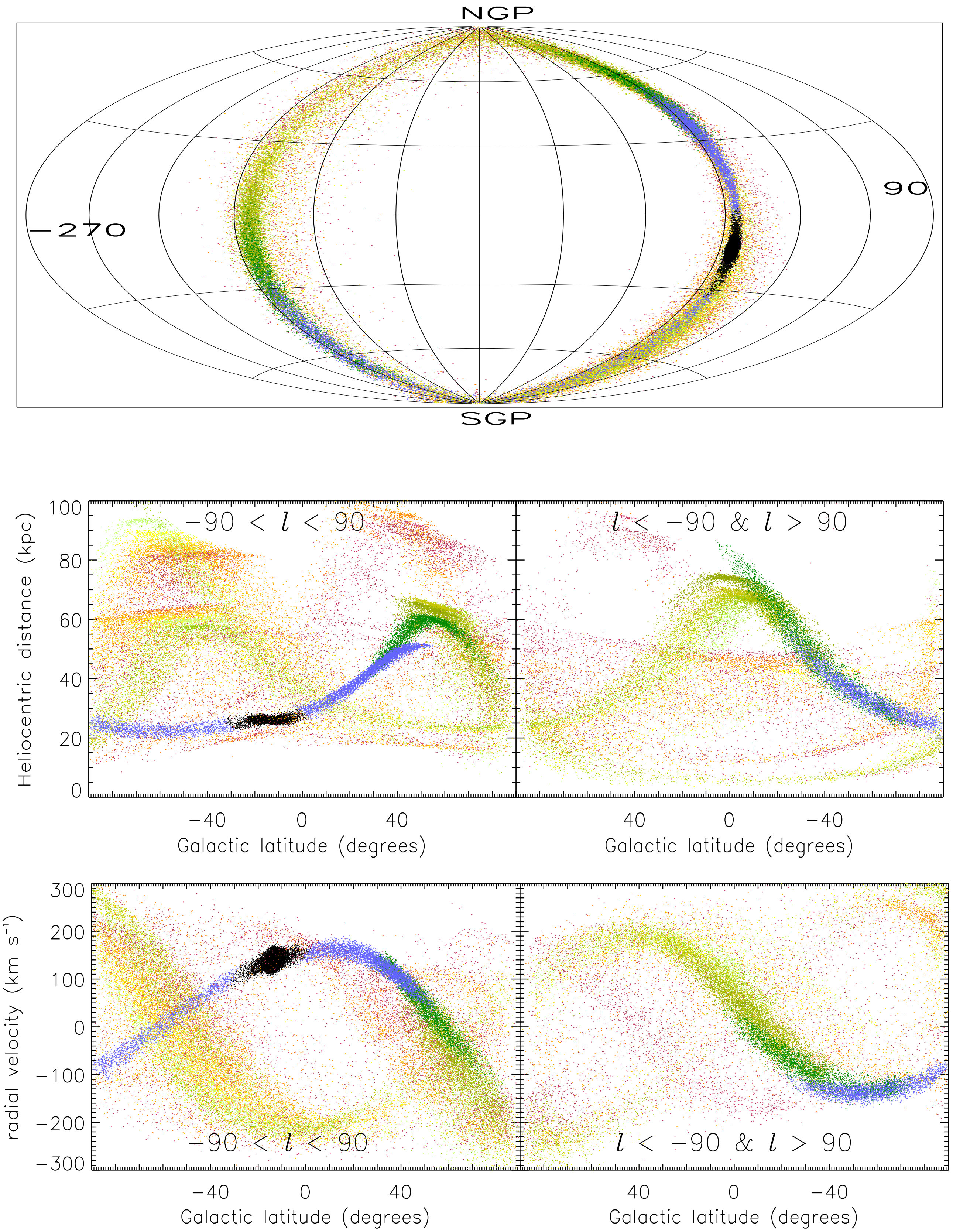

Figure 8. Top panel: Distribution in the sky (l, b) of the particles for our constant mass-to-light ratio model of Sagittarius after 12.5 Gyr. Different colours indicate material stripped off in different passages. **Central panel**: Heliocentric distance as a function of Galactic latitude, at the same time as the top panel, and with the same colour coding. Note that "streams" formed early on are wider than the more recent ones. **Bottom panel**: Heliocentric radial velocity as a function of Galactic latitude, at the same time and using the same colour coding as before.

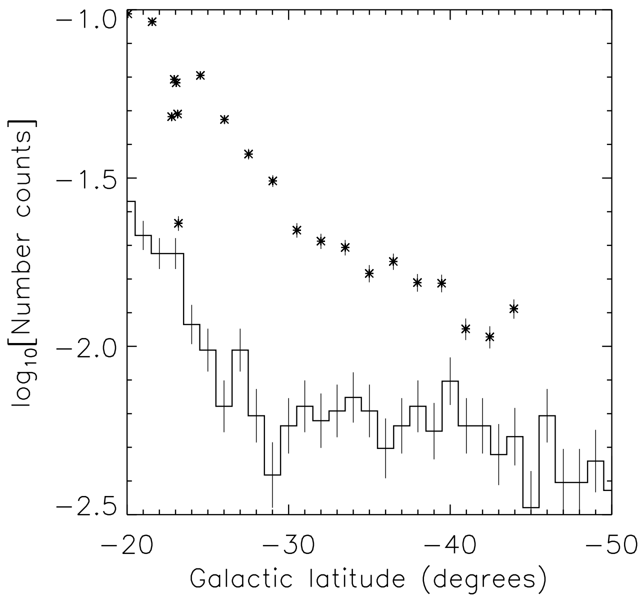

Figure 9. Number counts along the major of axis of the remnant system, outside its main body, within a strip of 3° to 10° in longitude. The error bars indicate Poissonian noise in the number counts. For comparison, we show the data by Mateo et al. (1998) arbitrarily shifted.

3.3.2.1 Outer Structure of Sagittarius. Mateo et al. (1998) have traced Sagittarius material out to 30 degrees from its nucleus: the globular cluster M54. They obtained deep photometric data along the southeast extension of the major axis of Sagittarius. In Figure 9 we show the particle counts in our simulation for the strip 3° to 10° in longitude, and spanning about 30° in latitude outside the main remnant body. For comparison we plot the data by Mateo and collaborators, shifted a few degrees in latitude, and arbitrarily offset in number counts. Thus qualitatively we reproduce the break in the number counts profile. This change in slope is indicative of the transition between material which is still bound today and that lost in the last pericentric passage.

3.3.2.2 Star counts at $b = -40°$. Majewski et al. (1999) have claimed a detection of a possible stream from Sagittarius at $b = -40°$ and $l = 11°$, at a slightly smaller heliocentric distance of 23 kpc and with a radial velocity of the order of $30\,\mathrm{km\,s^{-1}}$. As they discuss, this velocity may be strongly affected by contamination by other Galactic components. We note, however, that we would predict a stream of stars (shown in blue) going through this latitude and longitude with roughly the observed distance, and with a radial velocity of $55\,\mathrm{km\,s^{-1}}$. (See the central and bottom left panels of Fig. 8, $-90° \le l \le 90°$.). As mentioned above, this stream is formed mostly by material lost in the previous pericentric passage and not three passages ago, as in the model of Johnston et al. (1999). This difference reflects the different orbital timescales in the two models. The surface density of stars may be able to distinguish between them; it is predicted to be higher in our case.

Unfortunately, Majewski and collaborators could not detect the northern stream. They either did not reach the magnitude limit of 19.3^m expected for the red giant clump, or were offset by a few degrees from its expected location. Thus, for example, Majewski et al. (1999) had a limiting magnitude of ~ 21 at $b = 41°$ and $l = -6°$, but $V \lesssim 19$ at $b = 41°$ and $l = 6°$. The actual stream in our model is predicted to go through $l \sim 1°$ and to be about 2° wide. Note that the width prediction is more secure than the location since the motion of Sagittarius in the l-direction is poorly constrained at present, although a flattened halo would make the streams wider.

3.3.2.3 RR Lyrae found by the Sloan Digital Sky Survey. The Sloan Digital Sky Survey (SDSS) commissioning data has detected 148 candidate RR Lyrae stars in about 100 deg^2 of sky, along the celestial equator ($-1.27° \le \delta \le 1.27°$), and from $\alpha = 160.5°$ to $\alpha = 236.5°$ (Ivezic et al., 2000). Although the faint-magnitude limit of the SDSS would allow them to detect RR Lyrae stars to large Galactocentric distances, they find no candidates fainter than r*$\sim$ 20, i.e., farther than 65 kpc from the Galactic center. The distribution of stars in their sample is very inhomogeneous and shows a clump of over 50 stars at about 45 kpc from the Galactic centre, which is also detected in the distribution of nonvariable objects with RR Lyrae star colors.

By studying carefully Figure 8, and from our previous discussions, we are naturally led to believe this substructure could be associated with the northern streams of Sagittarius. In the upper left panel of Figure 10 we see how, in our simulations of Model I, a stream of material intersects the area observed by SDSS. The positions of the particles in our simulations are in excellent agreement with those of the RR Lyrae candidates belonging to the reported substructure. The upper right panel shows the visual magnitude of the particles falling in the region of the sky analysed by SDSS. We note here that there are basically two substructures in this region: one at $V \sim 19.5^m$, and a second one, at a fainter magnitude $V \sim 20.5^m$ (for $M_V = 0.7^m$ characteristic of RR Lyrae stars, e.g. Layden et al. (1996)). The first lump clearly could correspond to the substructure observed in the SDSS data. The material in this lump is mostly formed by particles that were lost in recent pericentric passages (i.e. 1 – 3 Gyr ago) as shown in the bottom left panel of Figure 10.

As Ivezic et al. (2000) discuss, they do not find any RR Lyrae stars fainter than $V \sim 20^m$. This would be in apparent contradiction with our results, (e.g. top right panel of Fig. 10). However, we need to estimate how much material we find in each lump, calibrate this number with respect to the number of RR Lyrae in the lump observed by SDSS, and thereby determine how many RR Lyrae SDSS could have missed. In the first lump we find 1264 particles, whereas the second has 362 particles. According to Ivezic et al. (2000) the detection efficiency decreases rapidly between $V \sim 20^m$, where it is fifty per cent, and $V \sim 21^m$ where it is zero. We here assume that for stars of $V \sim 20.5^m$ this efficiency is about 15%, which means that only 54 of the 362 particles could, in principle, have been observed. Therefore, we estimate that the ratio of unobserved to that of observed debris material is 0.043 in this region of the sky. Thus if SDSS found ~ 50 RR Lyrae belonging to the first substructure, it should have detected $\sim 2.14 \pm 1.46$ RR Lyrae in the fainter magnitude range. This means that the failure to detect fainter RR Lyrae in this region of the sky is barely significant in this context. From this perspective we cannot rule out that a second stream of debris material is located at much larger distances (typically between 80 and 100 kpc from the Sun, as shown in Figure 8).

Nevertheless the absence of a visible stream may be indicating that this material could be dark-matter dominated. This second stream is formed by particles that became unbound more than 7 Gyr ago. It therefore corresponds to particles orbiting the outskirts of the progenitor of Sagittarius. If this region of the system was dark-matter dominated, such streams would remain unobservable. Fainter data ($V \sim 20-21^m$) in this region of the sky could be crucial to constrain the initial properties of the system, e.g. size, total luminosity. This particular region of the sky should thus be explored further!

3.3.2.4 Carbon stars by the APM The APM survey has detected about 75 high latitude carbon giants presumably belonging to the halo. These stars being of intermediate age, could trace streams that have recently become unbound from Sagittarius or from other Galactic satellites. Ibata et al. (2000) have proposed that a large fraction of the observed halo carbon stars belong to Sagittarius tidal debris, since they preferentially occur near the great circle of its orbit. Even though there are large uncertainties in the determination of distances to these carbon stars, and the survey is not complete, particularly in regions where we expect Sagittarius streams to be present, this proposal clearly fits within the expectations for the models we have developed here.

4 CONCLUSIONS

We have found viable models for the Sagittarius dwarf galaxy with a wide range of total luminosities and masses, and both with and without extended dark halos. A purely stellar progenitor could be a King model with a total velocity dispersion of 18.9 $\mathrm{km\,s^{-1}}$, a core radius of 0.44 kpc and a tidal radius of 3 kpc. For the case where the progenitor is embedded in an extended massive halo, the initial stellar distribution follows a King profile with the same core radius, a slightly larger total velocity dispersion of $23\,\mathrm{km\,s^{-1}}$ and similar extent. The dark-matter is more extended. The data available at present only weakly constrain the total initial extent either of the light or of the mass. The observed metallicity data, for example, are consistent with an initial galaxy similar to either of our detailed models, both of which would lie within the scatter of the luminosity–size–velocity dispersion–metallicity distribution for more distant dwarf spheroidal galaxies in the Local Group. Thus we see no indication that Sagittarius is in any way anomalous. Further work on the debris streams of Sagittarius is needed to constrain better its initial total luminosity, and to distinguish between purely stellar or dark-matter dominated progenitors.

It is certainly encouraging that our models could reproduce the data available both on the main body and on the debris streams. We wish to stress however, that this does not mean that we have found the "ultimate" model. Other models with similar characteristics may also exist. Alternatives would include progenitors with smaller stellar masses or larger dark halos; flattened systems or with anisotropic velocity distributions; or systems with a stellar disk and a spherical dark halo (as proposed for the progenitors of dSph by Mayer et al. (2000)). Moreover, our assumption of a rigid Galactic potential, which does not vary in time over 12 Gyr, is clearly simplistic in view of current models for the formation of structure in the Universe. Only when we have a better estimate of the total luminosity of Sagittarius, both in its main body, as well as on its streams, we will be able to model it in greater detail. The present interest in the debris streams of Sagittarius will help us understand not only the properties of what has turned out to be just another dwarf spheroidal, but also the formation history of our Galaxy. A complete map of the streams will, for example, allow us to derive the Galactic potential (Johnston et al. 1999). If these streams are less smooth or broader than expected, this may indicate smaller scale structure present in the halo either now or when this was assembled.

ACKNOWLEDGMENTS

We thank Pavel Kroupa and James Binney for comments on earlier versions of this manuscript. We have enjoyed discussions with Heather Morrison and Paul Harding. CONICET, Fundación Antorchas, DAAD–Fundación Antorchas, and EARA are acknowledged for financial support.

REFERENCES

Bergbusch P.A., VandenBerg D.A., 1992, Ap. J. Suppl., 81, 163
Edelsohn D.J., Elmegreen B.G., 1997, MNRAS, 290, 7
Gómez-Flechoso M.A., Fux R., Martinet L., 1999, A&A, 347, 77
Helmi A., White S.D.M., 1999, MNRAS, 307, 495
Ibata R., Gilmore G., Irwin M., 1994, Nature, 370, 194
Ibata R., Gilmore G., Irwin M., 1995, MNRAS, 277, 781 (IGI95)
Ibata R., Wyse R.F.G, Gilmore G., Irwin M., Suntzeff, N.B. 1997, AJ, 113, 634 (I97)
Ibata R., Lewis G.F., 1998, ApJ, 500, 575
Ibata R., Irwin M., Lewis G.F., Stolte A., 2000, ApJL, in press (astro-ph/0004255)
Ivezic Z., Goldston J., Finlator K., et al. (for the SDSS), 2000, AJ, 120, 963
Jiang I., Binney J., 2000, MNRAS, 314, 468
Johnston K.V., Spergel D.N., Hernquist L., 1995, ApJ, 451, 598
Johnston K.V., Zhao H.S., Spergel D.N., Hernquist L., 1999, ApJ, 512, L109
Johnston K.V., Majewski S.R., Siegel M.H., Kunkel W.E., 1999, AJ, 118, 1719
King I.R., 1966, AJ, 71, 64
Klessen R., Kroupa P., 1998, ApJ, 498, 143
Layden A.C., Hanson R.B., Hawley S.L., Klemola A.R., Hanley C.J., 1996, AJ, 112, 2110
Majewski S.R., Siegel M.H., Kunkel W.E., Reid I.N., Johnston K.V., Thompson I.B., Landolt A.U., Palma C., 1999, AJ, 118, 1709
Mateo M., 1998, ARA&A, 36, 435
Mateo M., Olszewski E.W., Morrison H.L., 1998, ApJ, 508, L55
Mayer L., Governato F., Colpi M., Moore B., Wadsley J., Stadel J., Lake G., 2000, ApJL, in press (astro-ph/0011041)
Velázquez H., White S.D.M., 1995, MNRAS, 275, 23L
White S.D.M., 1983, ApJ, 274, 53
Zaritsky D., White S.D.M., 1988, MNRAS, 235, 289
Zhao H.S., 1998, ApJ, 500, L149

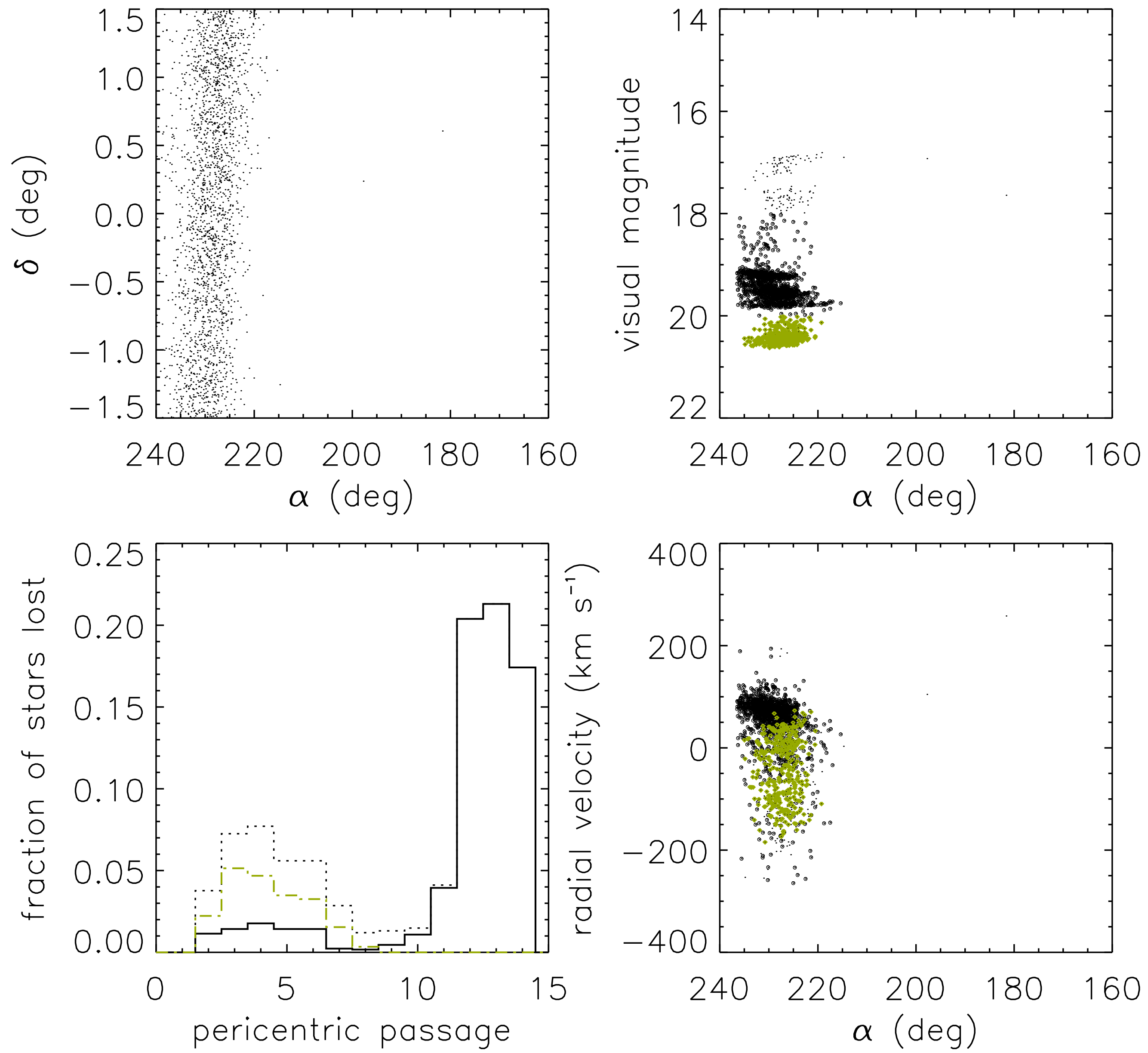

Figure 10. The top left panel shows the region of the sky analysed by the SDSS, where an excess of RR Lyrae has been observed. The top right panel shows the distribution in apparent magnitudes (i.e. distances for $M_V = 0.7^m$) of the particles in our simulations falling in that region of the sky. We have colour coded particles according to the range in distance: thick black dots correspond to $18 \leq V \leq 20$, lighter black dots to $V \leq 18$, and grey diamonds to $V \geq 20$. Note that the first group is strongly clustered around the magnitude range 19 – 19.5, as found by the SDSS for their RR Lyrae. The bottom left panel shows the distribution of pericentric passages (i.e. times) when the particles became unbound for each of the subgroups. The dotted histogram corresponds to all the particles present in this field of the sky. We note here that there are about twice as many particles which have been released in the last 3 Gyr, than earlier on. Most of the material in the first clump ($V \sim 19 - 19.5$) became unbound in the 12th to 14th pericentric passages, i.e. 1 – 3 passages ago. On the contrary all particles in the second clump ($V \sim 20.5$) became unbound in the first 7 passages. Finally the bottom right panel shows the radial velocity distribution with the same colour coding as before. We note that the stream appears rather diffuse in velocity space and strongly clustered in space because of the "bunching up" of the particles orbits that takes place near their apocentres.